# Nature-inspired synthetic oligourea foldamer channels allow water transport with high salt rejection

Chiranjit Dutta, Pannaga Krishnamurthy, Dandan Su, Sung Hyun Yoo, Gavin W Collie, Morgane Pasco, Jan Kazimierz Marzinek, Peter J. Bond, Chandra Verma, Axelle Grélard, et al.

# Nature-inspired synthetic oligourea foldamer channels allow water transport with high salt rejection

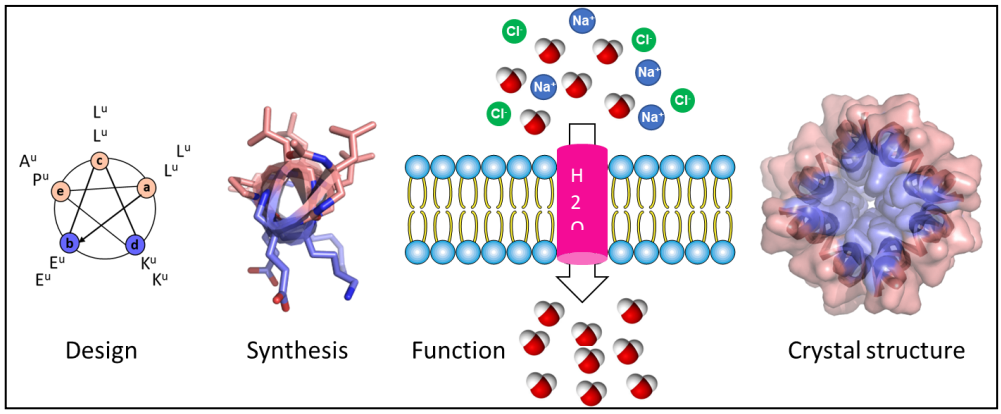


Short helical amphipathic oligourea foldamers were designed with distinct hydrophobic and hydrophilic faces. Two of the foldamers (**H2OC1**, **H2OC2**) obtained by solid phase synthesis self-assembled into channel-type nanostructures that show efficient water permeability across lipid membranes, while rejecting ions. A self-assembled quaternary structure with two superhelical scaffolds results in the formation of 4.8 and 6.4 Å inner pores that were observed in the crystal packing of **H2OC1**. Both pores have hydrophilic interior and hydrophobic exterior surfaces. Our findings demonstrate the channel forming ability of oligourea foldamers in lipid bilayers and such novel artificial water channels could be beneficial for water purification applications.

## Highlights

- Design of synthetic, self-assembling, helical oligourea foldamers that form artificial water channels
- Solid-state NMR experiments and molecular dynamics simulation suggest proper insertion of foldamers into lipid vesicles, without perturbations of the lipid phase, thermotropism and internal dynamics
- Oligomerization of the amphipathic foldamers leads to channel-type nanostructures in lipid membranes with selective, high water transport and ion rejection
- X-ray crystal structure shows a narrow (4.8 Å) hydrophilic pore in the superhelical assembly of a selected water transporting oligourea foldamer

# Nature-inspired synthetic oligourea foldamer channels allow water transport with high salt rejection

Chiranjit Dutta,[1,2] Pannaga Krishnamurthy,[1,2] Dandan Su,[3] Sung Hyun Yoo,[4] Gavin W. Collie,[5] Morgane Pasco,[4] Jan K. Marzinek,[6] Peter J. Bond,[7] Chandra Verma,[1,6,7] Axelle Grélard,[4] Antoine Loquet,[4] Jianwei Li[1], Min Luo[1], Mihail Barboiu,[3,*] Gilles Guichard,[4,*] R. Manjunatha Kini,[1,8,*] Prakash P. Kumar[1, 2,*]

Affiliations

[1]Department of Biological Sciences, National University of Singapore, Singapore, Singapore.

[2]NUS Environmental Research Institute (NERI), National University of Singapore, Singapore, Singapore.

[3]Institut Européen des Membranes Adaptive Supramolecular Nanosystems Group, University of Montpellier ENSCM, CNRS, Place Eugène Bataillon, CC 047, F-34095 Montpellier, France

[4]Univ. Bordeaux, CNRS, Bordeaux INP, CBMN, UMR 5248, Institut Européen de Chimie et Biologie, 2 rue Robert Escarpit, F-33600 Pessac, France

[5]Discovery Sciences, R&D, AstraZeneca, Cambridge, UK

[6]Bioinformatics Institute (A*STAR), 30 Biopolis Street, #07-01 Matrix, Singapore 138671, Singapore

[7]School of Biological Sciences, Nanyang Technological University, 60 Nanyang Drive, Singapore 637551, Singapore.

[8]Department of Pharmacology, Yong Loo Lin School of Medicine, National University of Singapore, Singapore.

[*]Corresponding authors – prakash.kumar@nus.edu.sg ; dbskini@nus.edu.sg ; g.guichard@iecb.u-bordeaux.fr ; mihail-dumitru.barboiu@umontpellier.fr

## SUMMARY

**Biomimetic membranes incorporating artificial water channels (AWC) are being developed for industrial water purification. Achieving high water permeation with salt rejection remains a challenge to be overcome while designing AWCs. Natural porins are the perfect examples of selective water transport through the cell membrane. Oligourea foldamers form predictable, helical structures that can be used to create similar biomimetic porin-like architectures. Here, we report the synthesis of amphipathic, helical oligourea foldamers that self-assemble to generate artificial channel-type nanostructures. Two of these foldamers (H2OC1, H2OC2) allow superior water permeability up to 88.7 µm/s across lipid membranes while providing almost total salt rejection. Solid-state NMR and cryo-EM experiments suggest proper insertion of foldamers into lipid vesicles, without perturbing the lipid phase, thermotropism and internal dynamics. The estimated per channel water transport of H2OC1 was 1.55 x $10^9$ $H_2O$/s. The H2OC1 crystal structure shows that oligourea helices pack together by hydrophobic and salt bridge interactions to build two channel-like assemblies. These channels differ in their hydrogen bonding patterns and result in hydrophilic pores of diameter 4.8 and 6.4 Å, respectively. Molecular dynamics simulation supports the experimental data on transport properties and suggests that H2OC1 can form a stable channel in lipid membranes. The selectivity of water and ions through foldamer assemblies is regulated at the sequence level. Ease of design, synthesis, purification, proteolytic stability, and microbial resistance of oligourea foldamers are added advantages. Our findings can help to develop novel AWCs for water purification applications.**

**Keywords:** Oligourea foldamers, supramolecular assembly, artificial water channels, desalination, water transport, stopped flow

## The bigger picture

Water scarcity is a global problem. Reverse osmosis is a costly and energetic water purification technology. Biomimetic membranes embedded with aquaporins (AQP) or artificial water channels (AWC) were developed to meet the industry needs. Although AQP exhibits high water permeability, its long-term stability is a limiting factor. We designed and synthesized helical amphipathic oligourea foldamers that can be used to generate artificial porins, as a new class of AWC. The chemical synthesis can be scaled up with sequence-based tunability of their properties. They self-assemble to form channel-type structures that exhibit selective water permeability across lipid bilayers. The crystal packing of one foldamer shows a superhelical assembly resulting in the formation of a porin-like superstructure with a hydrophilic pore of 4.8 Å diameter. The known resistance of oligoureas to proteolytic degradation could offer long-term stability indicating their suitability for water purification.

## INTRODUCTION

Fresh water scarcity currently affects over 4 billion people worldwide and is a growing challenge faced by humanity. High population, industrialization, deforestation and climate change lead to depletion and contamination of natural water resources, all of which increase the demand for fresh water.[1] Currently, reverse osmosis (RO) membrane and membrane distillation technologies are used to produce ~100 million tons of desalinated water per day from seawater.[1] However, the high energy consumption and overall cost of the existing technologies necessitate the search for better alternatives. In this regard, the aquaporins (AQPs) have been proposed as active components for the fabrication of desalination reverse osmosis bioassited membranes.[2] AQPs are transmembrane proteins that allow high water permeability (~$10^9$ $H_2O$ $s^{-1}$) across lipid membranes, while complete rejection of ions and protons.[3] The key structural feature of the AQP hydrophobic interior is a narrow 3 Å diameter pore, composed of a key asparagine-proline-alanine (NPA) motif, enabling transport of water molecules in a single-file.[3] Unfortunately, development of AQP-based membranes is limited by the long-term protein stability issues under harsh pressure and salinity RO conditions.[1,2]

Artificial water channels (AWCs), constructed from simple molecular components mimic the structures and functions of natural active protein channels. They address the drawbacks of AQPs and could be used to develop robust biomimetic membranes for the future.[2,4] Carbon nanotubes (CNTs) are among the most promising artificial nanostructures for the development of AWC.[5] Both wide- and narrow-diameter CNTs show high water permeability ($10^9$ and $10^{11}$ $H_2O$ molecules/channel $s^{-1}$) and they block anion transport, but not cations.[5] The single file water permeability of narrow-diameter CNTs exceeds AQP1 performance by a factor of 6. Indeed pore-lining residues in AQP1 can form H-bonds with incoming water molecules, thus transport rates are limited by kinetics of H-bond breakage and reformation, molecular reorientation.[5] In contrast, pore walls of CNTs cannot form H-bonds and allow unimpeded water transport.[5] Thus, the narrow diameter of CNTs promises selectivity as their hydrophobic interior permits water transport with low resistance.[6]

Another class of AWCs described is the imidazole-derived I-quartet channels[7] , which form tubular superstructures. These channels build a 2.6 to 2.8 Å pore similar to AQPs

and completely exclude ions except protons.[7,8] The reported water permeability through the I-quartet is $10^6$ to $10^7$ $H_2O$ $s^{-1}$ per channel in lipid bilayers[9] is promising and has been translated to planar polyamide membranes for desalination with high per area permeability of 2.5-3 LMH/bar while maintaining a high NaCl rejection of 99.8%.[10] Fluorous oligoamide nanorings of polytetrafluoroethylene self-assemble to create nanochannels through stacking[11]. Due to the water repellent property of carbon-fluorine bonds, the interior of these channels is hydrophobic and allows a high rate of water flow and negligible $Cl^-$ permeability.

Hydrazide-appended pillar[5]arene, PAH have also been employed to develop AWCs due to their unique tubular conformations.[12] Similarly, peptide-appended pillar[5]arenes (PAP[5]s) showed higher permeability ($10^7$ $H_2O$ $s^{-1}$).[13] However, the PAH and PAP[5] channels exhibit high ion permeability due to a larger pore diameter of 5 Å making them un-useful for the fabrication of desalination membranes.[13] Smaller peptide-appended hybrid[4]arene (PAH[4]) have been used to reduce the pore diameter and achieve salt rejection. They showed increased water permeability of $>10^9$ $H_2O$ $s^{-1}$ similar to AQP and exhibited undetectable ion permeability.[14] Overall the PAH[4] translocate water outside the channels and their water / salt permselectivity exceeds the requirement for desalination membranes for which the scale-up methods remains to be solved.[14]

Foldamers are synthetic polymers that tend to generate higher-order folded structures and have been employed for developing AWCs. Aromatic helical aquafoldamers, such as pyridine/oxadiazoles,[15–17] polypyridines,[18,19] polyhydrazides[20], and fluorofoldamer[21] show selective water and ion transport through their interior helical pore up to 2.7 x $10^{10}$ $H_2O$ channel $s^{-1}$ with salt rejection, exceeding to that of AQP1.[20]

However, to the best of our knowledge, there has been no attempt to create artificial water channels from sequence-defined proteinomimetic foldamers that are used as scaffolds that self-assemble into precise quaternary nanostructures with intrinsic porosity (*i.e.* self-assembled foldamer-based porin-like channels).[17-21] N,N'-linked oligoureas are a class of synthetic peptidomimetic foldamers which have been demonstrated to form well-defined helical structures in both organic and aqueous environment akin to regular peptide helices.[22] Amphipathic sequences with a patch of hydrophobic side chains at the surface of the helix have been shown to self-assemble into various quaternary structures including

nanotubular structures.[23–25] These oligourea sequences were synthesized using solid-phase techniques akin to peptide synthesis, from enantiopure activated monomers prepared from amino acid derivatives (building blocks, BB).[22,26] The BBs were protected on one side as azides and activated at the other extremity as succinimidyl carbamates (e.g., $N_3$-Leu$^U$-OSu). In contrast to natural peptides, these foldamers are substantially more resistant to proteolytic degradation due to their oligourea (*i.e.* non amide) backbone.[27] These different properties make them potential candidates for synthesizing AWCs.

Here, we report the successful design and synthesis of amphiphilic oligourea foldamers, which are able to form transmembrane channels exhibiting high water permeability rejecting all ions. We show that these non-natural oligomers form tunable helical scaffolds self-assembled in Porin-like nanostructures. The state of oligomerization was investigated by mass spectrometry and transmission electron microscopy (TEM). The molecular insertion into lipid vesicles was investigated by solid-state NMR spectroscopy. We further characterized their water and ion permeability properties in lipid vesicles. Also, we present their three-dimensional structures elucidated by X-ray crystallography. The high-water permeability coupled with resistance to proteolytic degradation makes these novel synthetic foldamers possible candidates for industrial water purification applications.

## RESULTS AND DISCUSSION

### Design and synthesis of H2 derivatives

To design transmembrane water channels, we designed **H2OC1**-**H2OC4** scaffolds starting from known self-assembling properties of a previously reported amphipathic helical oligourea foldamer named **H2**.[23,24] The 10-mer **H2** showed extended superhelical structure with two right-handed intertwined superhelices that form a channel in aqueous conditions with hydrophilic interior and a pore diameter of *ca* 17 Å due to its global amphipathicity.[23] The oligourea sequence, composed of two pentad repeats, has been designed to form an amphipathic helix with an extended hydrophobic face using the following principles. At positions 'a' and 'c': four leucine-type urea residues ($Leu^U$) (two in each pentad repeat); at position 'e': proline-type ($Pro^U$) residue in the first pentad and alanine-type ($Ala^U$) in the second pentad (Figure 1A).

These hydrophobic residues at the exterior surface assist in forming a dense and precise packing during self-assembly of **H2**. Additionally, the side chains of four charged residues (two glutamate-type side chains ($Glu^U$) at position 'b' and two lysine-type side chains ($Lys^U$) at position 'd') point into the lumen and form a highly charged interior of the channel. The electrostatic interactions and salt-bridges play a major role in the formation of intricate H-bonding network among proximal and distal oligourea residues and contribute to stabilize the overall packing.

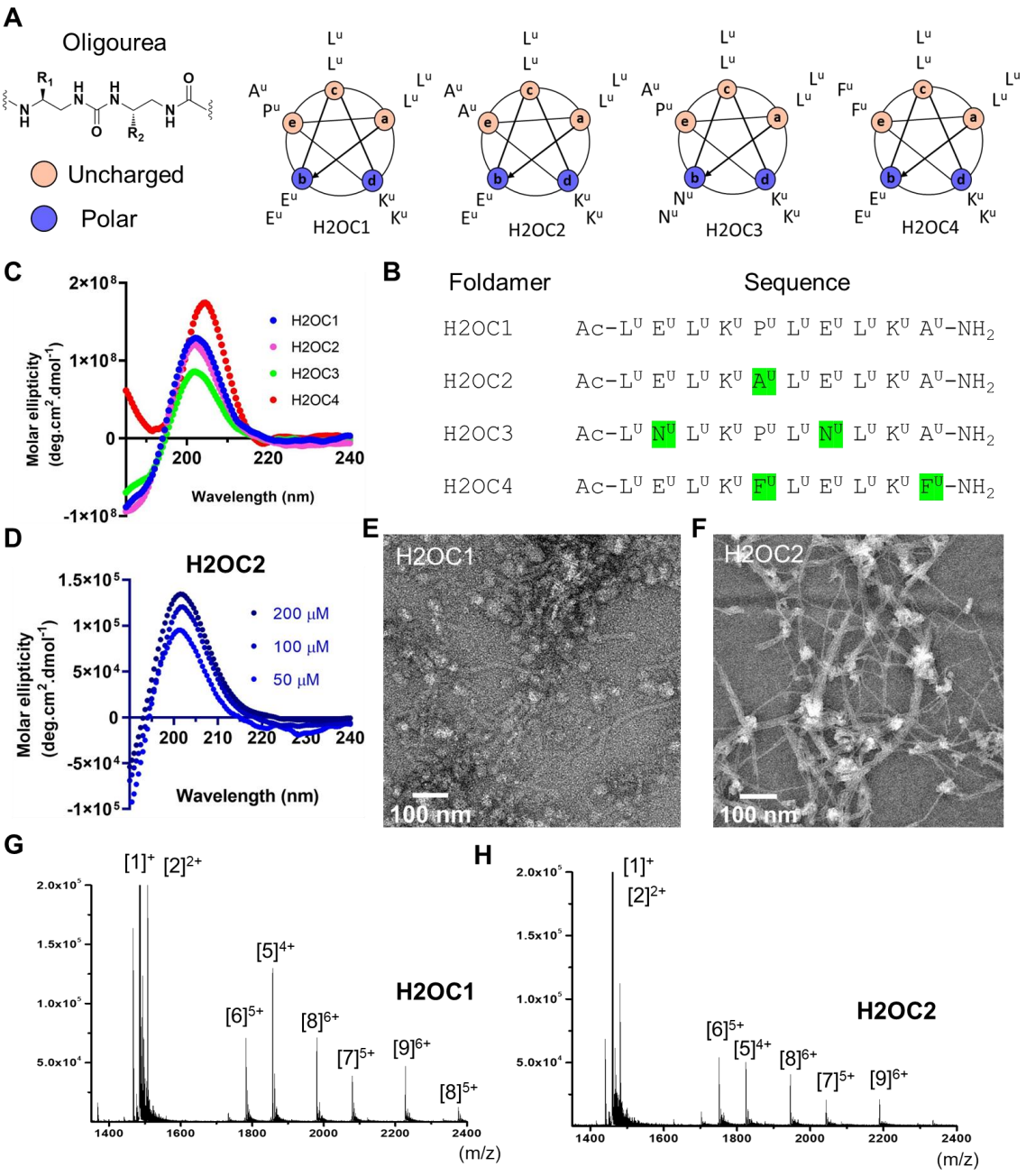


**Figure 1. Molecular design and biophysical characterization of oligourea foldamers**
(A) Helical-wheel representations of designed **H2** variants showing side-chain distribution of oligourea residues in pentad. Polar and charged residues, and uncharged residues are depicted as salmon red and cyan blue, respectively.
(B) Sequences of synthesized amphipathic oligourea foldamers **H2OC1**, **H2OC2**, **H2OC3** and **H2OC4**. Highlighted residues represent the point mutation to **H2OC1**.
(C) Circular dichroism (CD) spectra of oligourea foldamers show a peak at ~202 nm indicating their helical conformation.
(D) CD spectra of **H2OC2** in water exhibit concentration-dependent increase of molar ellipticity at ~202 nm.

(E,F) Negative-stained transmission electron micrographs of (E) **H2OC1** and (F) **H2OC2** revealed self-assembled morphologies at 200 μM in 10 mM HEPES buffer, pH 7.0. They showed fiber-like networks packed in large knotted bundles (**H2OC2,** diameter ranging from 12.4 to 40.0 nm) and distinct fibers (**H2OC1,** diameter 5.5±0.6 nm).
(G,H) Electrospray ionization (ESI) mass spectrometry profiles of (G) **H2OC1** and (H) **H2OC2**. The ESI spectra reveal distribution of heterogeneous multimeric species of oligoureas. The isotopic peak at m/z value of 1856.76 of **H2OC1** indicates pentameric species ($[5]^{4+}$). Other isotopic peaks of multimers are also identified.

We designed and synthesized a series of close **H2** analogues and carried out their structural and functional analyses (Figure 1, S1-S5 and Table S1). In the first analogue, **H2OC1**, the N-terminal isopropyl group of **H2** was replaced by an acetyl group and the C-terminal methyl urea was replaced by a simple urea termination to reduce the hydrophobicity (Figure 1A-1B). To understand the local constraining effect of $Pro^{U}$, we prepared a second analogue **H2OC2** in which $Pro^{U}$ is replaced with $Ala^{U}$ at position 'e' (Figure 1A-1B). We have shown that $Pro^{U}$ does not interfere significantly with the helicity of oligoureas[23] unlike Pro in peptide chains.[28] In **H2OC3**, we replaced two $Glu^{U}$ with the less hydrophilic $Asn^{U}$ at the 'b' sites of pentads (Figure 1A-1B). Such substitutions were intended to reduce the interaction with water in the polar channel and facilitate faster water flow.[3,29] To enhance the penetration into lipid bilayers, we designed the analogue **H2OC4** by replacing $Ala^{U}$ and $Pro^{U}$ residues with $Phe^{U}$ at position 'e' in both pentads of **H2OC1** (Figure 1A-1B). Such aromatic Phe-type residues might favorably interact with fatty acyl chains and lipid head groups.[30] All oligourea foldamers were synthesized on a solid-support using microwave assistance (Scheme S1, Table S1 and Figures S2-S5) and purified according to previously established procedures.[23,31]

## Biophysical characterization of foldamers

The secondary structure and self-assembly of the foldamers were first investigated by circular dichroism (CD). All spectra showed a maximum at ~202 nm (Figure 1C-1D and S6), indicating helical conformation of **H2OC1** to **H2OC4** analogues at 100 μM in water[23,31]. They exhibit helicity even at lower concentrations. Concentration-dependent CD experiments of foldamers showed increased molar ellipticity with increasing foldamer concentration, indicating self-assembly in water (Figure 1D and S6).[23,31]

Negative-staining TEM studies of **H2OC1** and **H2OC2** showed the formation of extensive fiber networks in aqueous condition (Figure 1E-1F). **H2OC2** showed large fiber bundles with knots (with diameters ranging from ~12 to ~40 nm) consisting of protofilaments with diameter of 3.7 ± 0.8 nm, whereas **H2OC1** showed untangled fibers with a diameter of 5.5 ± 0.6 nm (Figure 1E-1F). The TEM observations support their fiber-like self-assembly.[23,24] In contrast, **H2OC3** showed vesicle-like morphology with

about 24 to 33 nm diameter (Figure S7A). **H2OC4** formed longer filaments with about 132 to 156 nm width (Figure S7C). The stoichiometry of oligourea foldamer self-assemblies was next investigated by mass spectrometry. ESI-MS analyses revealed the presence of discrete multimeric species[23,31] ranging from pentamer to nonamer of **H2OC1** and **H2OC2** in aqueous condition (Figure 1G-1H). In contrast, **H2OC3** showed a predominant pentameric species (Figure S7B). The TEM and ESI-MS results are thus consistent with **H2OC1**, **H2OC2** and **H2OC4** forming helical tubes as previously reported for **H2.**[23]

## Molecular insertion of foldamer channels into lipid vesicles

To investigate whether **H2OC1** and **H2OC2** foldamers have the molecular properties to be stably inserted into lipid membranes, we employed solid-state NMR spectroscopy to measure biophysical parameters in a lipid environment. Lipid vesicles composed of a mixture of phosphatidylcholine (PC) and phosphatidylserine (PS) (molar ratio of 4/1) were reconstituted in the presence of **H2OC1** and **H2OC2** at a molecule-to-lipid ratio of 1/20. To monitor the impact of foldamer insertion into the lipid vesicles, we first used $^{31}$P solid-state NMR to probe the lipid phase and membrane curvature effect. PC/PS vesicles exhibited a $^{31}$P spectral pattern characteristic of a lamellar lipid phase. $^{31}$P experiments carried out for vesicles containing **H2OC1** and **H2OC2** showed a comparable asymmetric spectral profile and a similar chemical shift anisotropy (Figure 2A), indicating that the lipid phase and the membrane curvature of the vesicles were not significantly impacted by the molecular insertion of the foldamers. To monitor the insertion of foldamers into the hydrophobic part of the lipid bilayer, we used $^{2}$H solid-state NMR on PC/PS vesicles for which the PC acyl chains were deuterated. We detected comparable $^{2}$H quadrupolar couplings for control vesicles and vesicles incorporating **H2OC1** and **H2OC2** (Figure 2B).

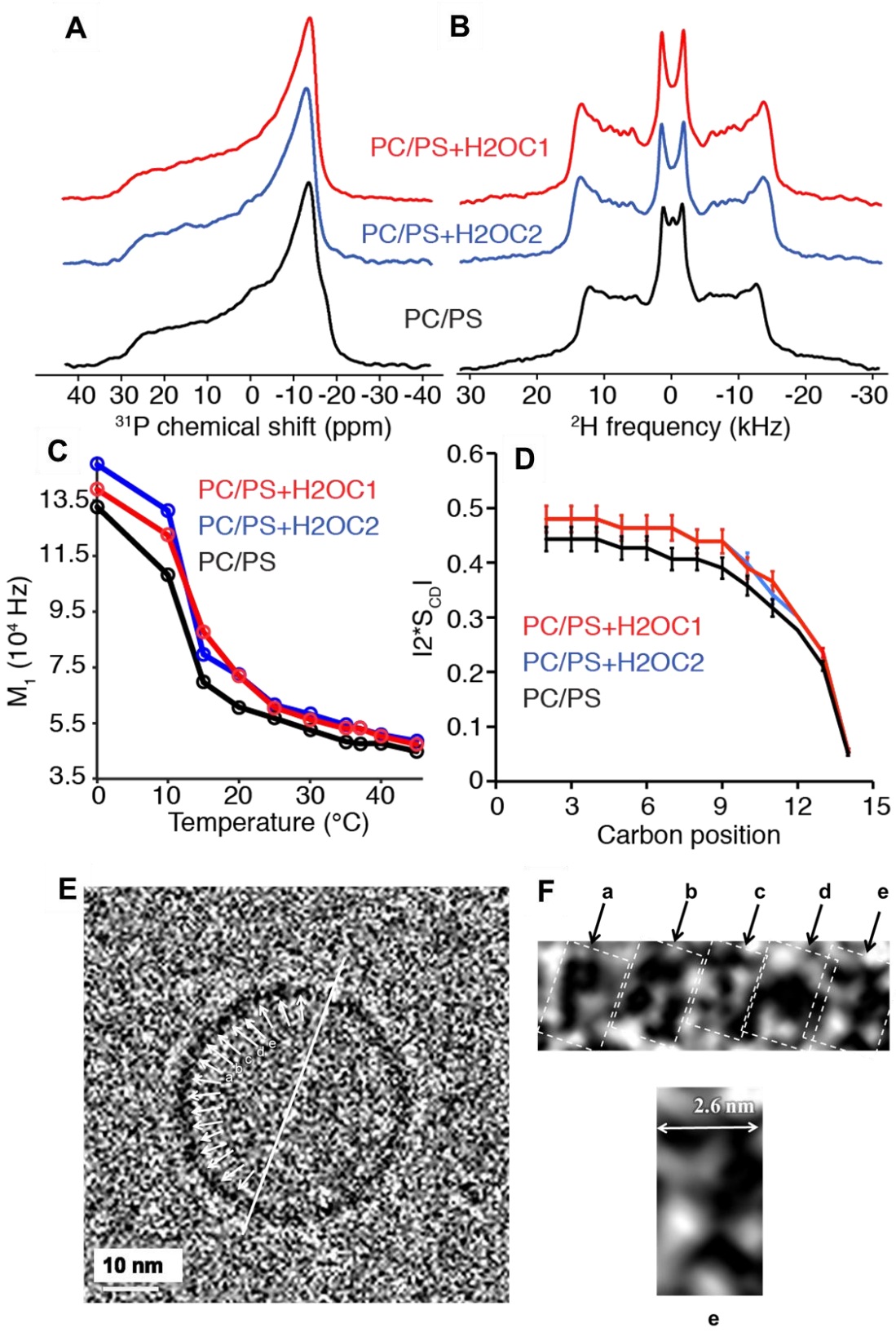


**Figure 2: Biophysical properties of foldamer insertion into liposomes** and cryo-EM images of H2OC1-embedded PC/PS (4:1) liposomes

(A) $^{31}$P static solid-state NMR experiments performed at 303K on PC/PS control vesicles (black) and PC/PS vesicles incorporating **H2OC1** (in red) and **H2OC2** (in blue).
(B) $^{2}$H static solid-state NMR experiments performed at 303K.
(C) Thermal variation of the first spectral moment $M_1$ of PC lipids as measured by $^{2}$H solid-state NMR.
(D) C-$^{2}$H order parameter as a function of labeled lipid carbon position.
(E) Self-assembled channels of **H2OC1** in a liposome. The location of channels in the membrane is highlighted with white arrows. The diameter of the liposome at the imaging plane is 55.3 nm.
(F) Magnified image shows the array of channels (e.g., a, b, c, d, e) in the lipid bilayer. The outer diameter of individual channels is 26 Å, compared to 29 Å in the crystal structure of **H2OC1**.

Since $^{2}$H quadrupolar couplings are related to the molecular orientation and the dynamics of the C-$^{2}$H bonds, this suggests that the foldamer insertion has a negligible effect on the internal lipid dynamic at the level of the acyl chain. Lipid thermotropism was evaluated by monitoring the $^{2}$H first spectral moment as a function of the sample temperature (Figure 2C). We observed that the melting temperature ($T_m$ = 285 K) of PC/PS liposomes stay the same in the presence of the **H2OC1** and **H2OC2** foldamers. Using spectral deconvolution, individual $^{2}$H quadrupolar splittings were employed to derive the lipid order parameters along the PC acyl chain (Figure 2D) that span half of a bilayer. Control PC/PS liposomes exhibited a characteristic profile of $S_{CD}$ order parameters with a plateau for carbons near the membrane surface and having a high structural order, followed a decreased of order parameters towards the mobile methyl carbon C14. We observed a similar profile for liposomes incorporating **H2OC1** and **H2OC2**, with a slight increase of $S_{CD}$ order parameters in presence of the foldamers, suggesting that their insertion slightly increases lipid acyl chain ordering. Taken together, solid-state NMR experiments suggest a proper and stable insertion of foldamers into liposomes, without perturbations of the lipid phase, thermotropism and internal dynamics.

Further, we employed cryo-electron microscopy (cryo-EM) to estimate the number of **H2OC1** channels within a unit area of the liposome membrane. The cryo-EM image shows that the foldamer channels were inserted in an orderly fashion without perturbating the lipid phase. The individual channels were 26 Å wide, and about 50 channels were present in a measured plane of ~174 nm circumference of the liposome (Figure 2E-F). This corresponds to 73046 channels per µm$^2$ at 1:100 (foldamer to lipid) molar ratio.

## Water permeability of porin-type foldamer channels

We measured the water permeability in lipid bilayers using a stopped-flow method to capture fast kinetics on the millisecond time scale of water efflux from liposomes led by osmotic pressure difference was determined by monitoring the change in the light scattering intensity of the liposomes.[4,5,32–34] (Figure 3A). We quantified the water permeability by the shrinkage mode, measured in PC/PS (4:1) liposomes. The foldamer-embedded liposomes were exposed to hypertonic osmolytes (sucrose and NaCl) (Figure 3A-3B). Interestingly, all four foldamers showed significant water permeability in the presence of sucrose or competitive ionic NaCl used as osmolytes (Figure 3B and S8-S9). **H2OC1 and H2OC2** showed the highest water permeability compared to other sequences (5- to 7-fold increase in water transport at 1:50 ratio over the control vesicles without the foldamers) (Figure 3B). Additionally, these foldamer channels showed comparable water permeability to that of gramicidin A (gA),[27,29], a natural ionophore, which transports water and cations across the membranes (Figure 3B and S8-S9).

The high-water permeability of **H2OC2** encouraged us to study the foldamer in more detail. Variation in lipid composition exhibits different properties of lipid membranes including charge, fluidity, and lateral pressure profiles.[36] Therefore, changes in lipid composition affect the interaction of lipids with extraneous compounds. The initial step of binding of cationic molecule to anionic lipid PS-containing membranes occurs by electrostatic interactions.[36] Therefore, the effect of different PC/PS ratios in liposomes on water permeability of **H2OC2** was evaluated (Figure S10). We observed no detectable water permeability in the presence of pure PC. However, with increasing PS concentration, the permeability increased until PC/PS ratio reached 4:1. Further increase in PS concentration for **H2OC2** resulted in decreased water permeability (Figure S10). The 10-residue oligourea foldamers consist of polar $Lys^{U}$ and $Glu^{U}$ residues. The ionic nature of these residues facilitates binding to membranes through electrostatic interactions. Further, the inclusion of anionic lipid PS in the membrane increases the electrostatic interactions with the foldamers. The insertion of foldamers in the membrane is further facilitated by their external hydrophobic surface.

Subsequently, **H2OC2** and PC/PS liposomes were mixed to obtain foldamer/lipid molar ratios from 1:1000 to 1:50 in 10 mM HEPES buffer, pH 7.0 and measured their water permeability.

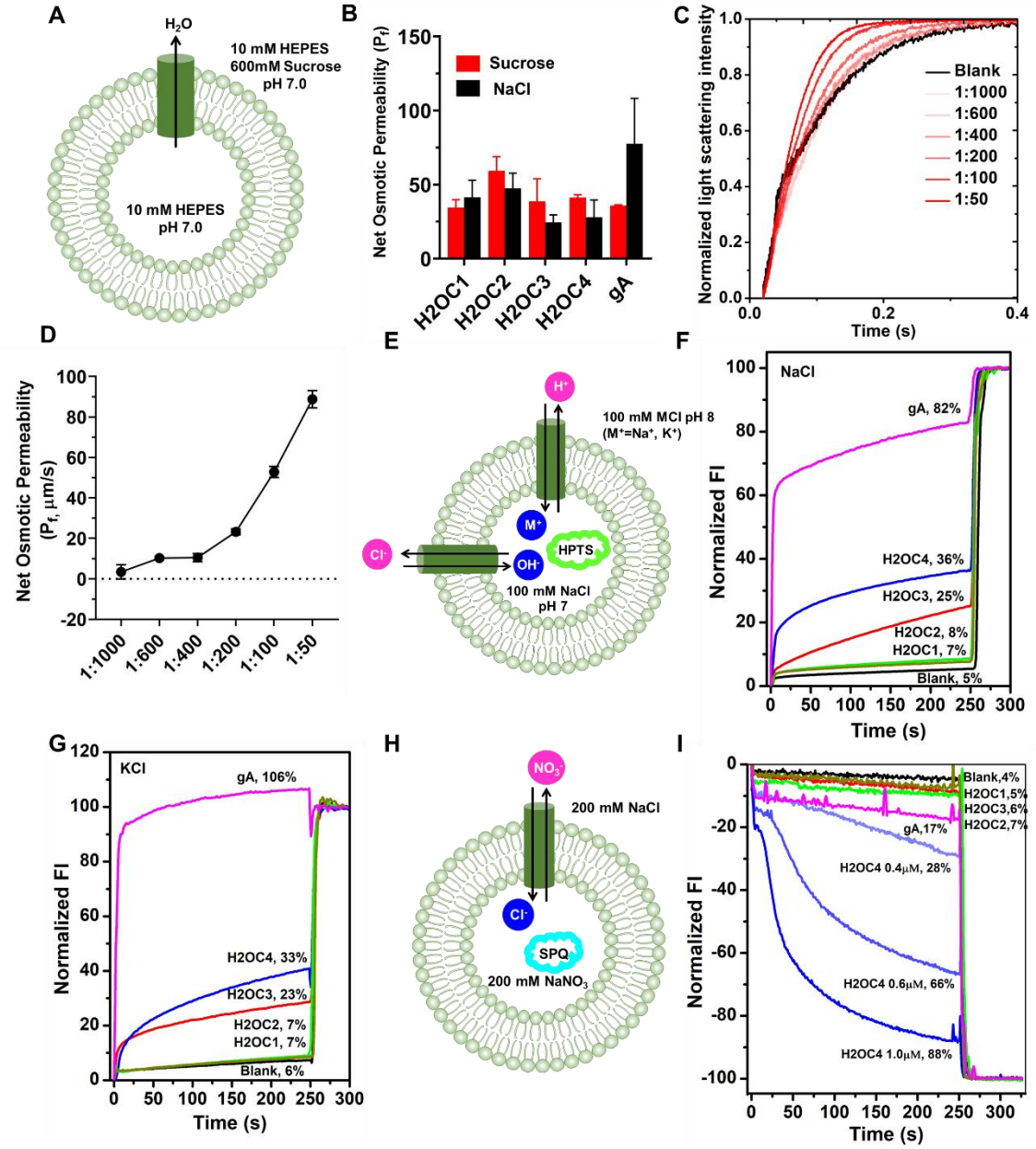


**Figure 3. Measurements of water and ion transport through oligourea foldamers**

(A**)** Schematic representation of water permeability measurement through foldamer channels in phosphatidylcholine/phosphatidylserine (PC/PS) liposomes suspended in a hypertonic osmolyte (600 mM sucrose).

(B) Stopped-flow analysis of oligourea foldamers showing water permeation through foldamer channels in PC/PS (4:1) liposomes.

(C**)** Light scattering traces of **H2OC2** embedded in PC/PS liposomes with different molar ratios showing an increasing water permeability with increased channel concentration when suspended in hypertonic osmolyte (600 mM sucrose). Curves were fitted with stretched function $y=c+a\exp(-Kx^b)$ to obtain exponential coefficients (K).[30-32]
(D**)** Water permeability through **H2OC2** channel measured at different channel densities exhibited a jump in permeability when lipid/channel molar ratio reached 100:1 to 50:1 indicating a possible cooperativity.
(E**)** Schematic representation of HPTS based fluorescence assay under high ionic gradients (100 mM NaCl and KCl). HPTS=8-hydroxypyrene-1,3,6-trisulfonic acid**.**
(F and G) salt rejections by **H2OC1** and **H2OC2** compared to natural ionophore gramicidin A (gA) and foldamers **H2OC3** and **H2OC4**.
(H**)** Schematic representation of chloride-selective, SPQ dye-based, fluorescence assay for ion transport.
(I**)** Chloride-selective ion transport by SPQ fluorescence quenching assay showed rejection of chloride ion by **H2OC1**, **H2OC2** and **H2OC3**. Concentration-dependent fluorescence quenching was observed with **H2OC4,** indicating chloride transport by **H2OC4**.

The light scattering intensity increased with exposure to an equal volume of hypertonic osmolyte (600 mM sucrose) with the increasing foldamer ratio (Figure 3C-2D). This indicates that increasing the molar ratio results in effective increase in incorporation of foldamers into the liposomes, leading to enhanced water permeation. The calculated water permeability ($P_f$) values of **H2OC2** vary from 10.5 µm/s (foldamer/lipid 1:400), 23.2 µm/s (@1:200) to 88.7 µm/s (@1:50) (Figure 3C-3D), close or superior to water permeability observed with gramicidin A (gA) channels. **H2OC2** also showed water permeability in the presence of other osmolytes such as glycine and glucose (Figure S11). Furthermore, the water permeability at pH 4.5 was lower than that at pH 7.0.

Based on the dimensions of the channels and liposomes, the theoretically calculated number of channels per liposome was 11 (see Suppl Info xxx). From the cryo-EM data we calculated the channel number to be 367 per liposome (for 1:100 molar ratio where 135 µM of **H2OC1** was used in 13500 µM PC/PS). However, the water permeabilities were measured by stopped-flow assays using 5 µM of **H2OC1** in 500 µM PC/PS (equivalent of 13.5 channels for 1:100 molar ratio per liposome). Thus, the single-channel water permeability of **H2OC1** was $1.55 \times 10^9$ water molecules/s, which is similar to the reported value for the natural aquaporin water channels. The calculated single-channel water permeability of **H2OC2** was $x.xx \times 10^9$ water molecules/s.

## Proton/ Ion transport properties of foldamers

High selective water transport is the most important feature for an AWC. Another crucial feature that is equally important for water purification is its ability to reject ions transport.[32,33] Therefore, we determined the ion transport properties of our selected foldamers in PC/PS (4:1) liposomes using standard fluorescence based HPTS assay (Figure 3E). The HPTS loaded liposomes were incubated with the foldamers for 5 min. before the experiments. A base pulse (20 µl of 0.5 N NaOH) was given at 50 s of the measurement to increase the external pH from 7.0 to 8.0. The natural ionophore gA, a monovalent cation selective channel[27,29] was used as a positive control (Figure 3F-3G). The changes in fluorescence intensity showed that **H2OC3** (36%) and **H2OC4** (25%) channels can moderately transport $Na^+$ and $K^+$ ions. However, the ion transport facilitated by the foldamers was much lower than that of gA (Figure 3F-3G). Interestingly, no detectable ion transport activity was observed for **H2OC1** (7%) and **H2OC2** (8%) in the presence of NaCl and KCl (Figure 3F-G). In addition, **H2OC1** and **H2OC2** foldamers are able to reject the divalent ions (Figure S12). This indicates strong salt rejection ability of these two foldamers. Therefore, they are suitable for water purification applications.

The chloride permeation through **H2OC1** and **H2OC2** channels was further investigated using chloride-selective dye 6-methoxy- N-(3-sulfopropyl) quinolinium (SPQ)[33,34] trapped in PC/PS (4:1) liposomes containing intravesicular $NaNO_3$ and extravesicular NaCl (Figure 3H). Oligourea **H2OC1**, **H2OC2** and **H2OC3** did not show any detectable chloride transport (Figure 3I). However, concentration-dependent quenching of fluorescence intensity was observed for **H2OC4** due to the influx of $Cl^-$ ions (Figure 3I). Collectively, these assays confirm the ion rejection properties of **H2OC1** and **H2OC2**.

The proton transport activity of oligourea foldamers were evaluated by the patch-clamp experiments[29,35] in PC:PS (4:1) and DOPC liposomes (Figure S13-S17). The proton conductance rates of **H2OC1** ($\gamma_{H^+}$ =7.4 pS) and **H2OC2** ($\gamma_{H^+}$ =25.8 pS) showed differences in PC:PS liposomes (Figure S13), but the values did not differ significantly in DOPC liposomes (Figure S1). **H2OC1** presents a better channel shape, longer retention time and higher channel opening probability at both lipid conditions (Figure S13-S14). Along with the water transport activity, we can speculate that protons are transferred

overall along water wires. Patch clamp single channel current traces and I-V plots of **H2OC1** and **H2OC2** recorded in symmetrical solutions (*cis* chamber = *trans* chamber = 1 M KCl solution) and asymmetrical solutions (*cis* chamber = 1 M KCl solution, *trans* chamber = 1 M NaCl solution) using DOPC and PC/PS (4:1) lipids show no obvious channel activity confirming the previously observed lack of ion transport ability by **H2OC1** (Figure S15 and S17A) and **H2OC2** (Figure S16, and S17B). **H2OC1** and **H2OC2** showed extremely low channel current (<5 μA). The observed channel opening under high voltage could have occurred due to ion polarization, which is not characteristic of ion transporters.(Ref?) Hence, calculation of single-channel ion permeability is not feasible here.

## Self-assembled channel structure of foldamer

An X-ray crystal structure of foldamer **H2OC1** at a high-resolution of 1.2 Å was determined in order to provide atomic-scale details of channel formation *via* self-assembly. (Figure 4, S18-S20, and Table S2-S3). The monomers exhibit the design-imposed amphipathic helical conformation consisting of distinct hydrophobic and hydrophilic faces (Figures 1A, and 4A) similar to those formed from **H2** (Figure S18 and table S3) ([23]). Crystal packing revealed oligourea helices forming a self-assembled superhelical channel-type assembly (Figure 4B).

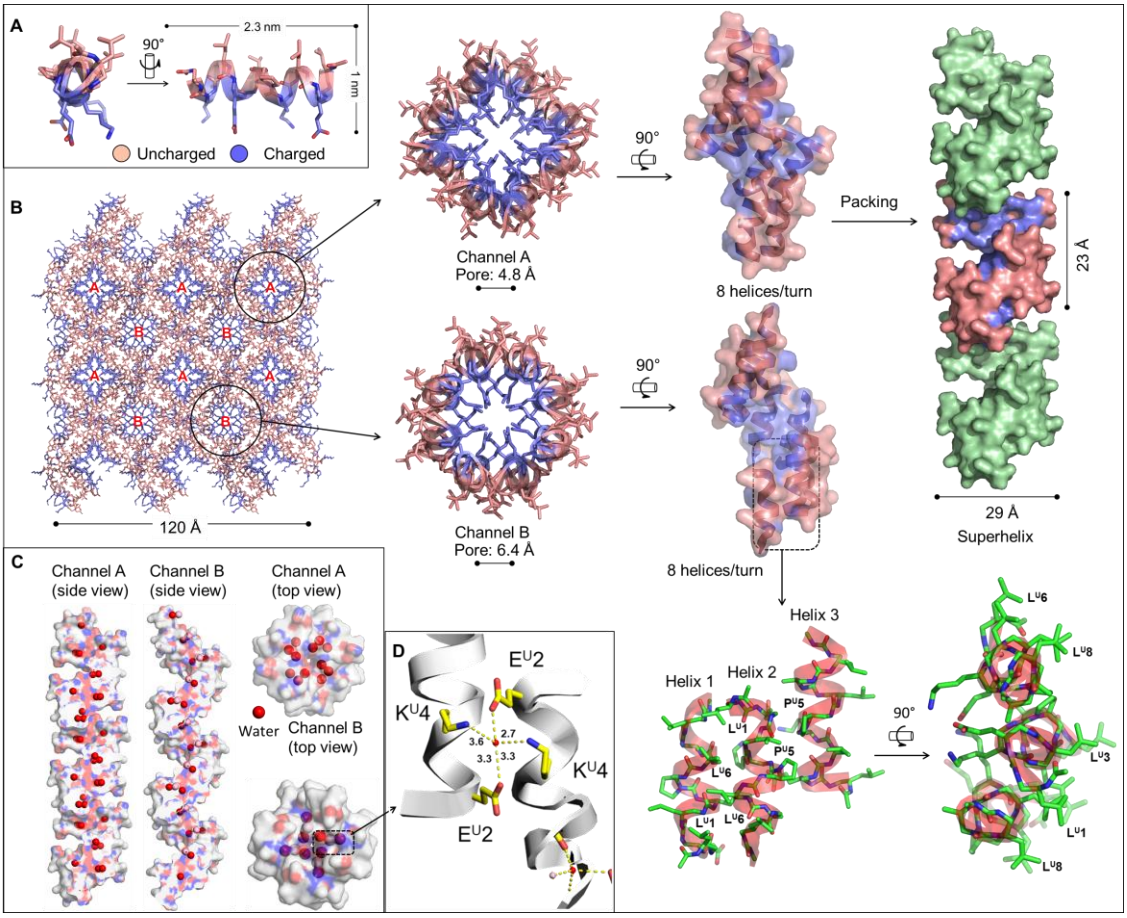


**Figure 4. Crystal structure revealing quaternary structure of foldamer H2OC1**
(A) Crystal structure of **H2OC1** shows a helical conformation of the monomer with a distinct hydrophobic (salmon red) and hydrophilic (blue) surfaces.
(B) Crystal packing shows two distinct channels (channel A and channel B). In this structure, channel B is formed in the interspace of four channel A assemblies. Both channels are packed through hydrophobic interactions of exterior surfaces. In the channel assembly, eight monomeric oligourea helices per turn are packed laterally. The neighboring helices are in an antiparallel orientation within the superhelical structure. Interior of both channels are composed of hydrophilic residues, creating a charged nanopore, while hydrophobic residues line the exterior.
(C) Water molecules that are H-bonded with the foldamer are shown as red spheres in the pores of channels A and B. Water molecules that do not form any H-bonding with foldamer helices are represented as pink spheres. Only selected water molecules are displayed.
(D) Water molecules in the pore form a H-bonding network with charged residues, $Glu^U$ and $Lys^U$. Hydrogen bonds show O-O and N-O distances of 2.7 and 3.6 Å, respectively. Images were created using PyMOL.

Two distinct channels can be identified in the crystal structure of **H2OC1**, namely channels A and B with an external diameter of 29 Å each (Figure 4B), which is close to

the dimensions observed in the cryo-EM images. These channels show apparent pore diameters of 4.8 and 6.4 Å, respectively. In channel B, the electron density maps for C-terminal $Lys^{U}9$, and $Ala^{U}10$ residues are not 'visible' leading to overestimation of its pore size. In both channels, the exterior surface is composed of the hydrophobic residues $Leu^{U}$, $Ala^{U}$, $Pro^{U}$ located at positions 'a', 'c' and 'e' in the helical-wheel representation. The pore of the channels is lined by the hydrophilic residues $Glu^{U}$ and $Lys^{U}$ situated at positions 'b' and 'd' (Figure 4B). Eight oligourea helices per turn associate laterally in a right-handed, staggered, antiparallel orientation by hydrophobic and electrostatic interactions within the superhelical structure. The intricate H-bonding network of salt-bridges between neighboring oligourea helices greatly contributes to stabilize the pore structure. The hydrophilic pore is hydrated with both H-bonded (to the $Glu^{U}$ and $Lys^{U}$ side chains) and mobile water molecules (Figure 4C-4D and S19-S20). A single turn (23 Å) could span across phospholipid membranes. Surprisingly, the crystal packing also revealed the presence of distorted helices that fill the void spaces between channel assemblies. These helices with a kink near the $Pro^{U}$ and $Lys^{U}$ residues are situated externally, defining four corners surrounding both channel assemblies (Figure S21). The well-defined self-assembled helical tubular structure of **H2OC1** in the crystal (Figure 4B) may suggest a model of interaction between the hydrophobic face of amphipathic foldamer helices and the hydrophobic component of lipid membranes compatible with the formation of pore in the lipid membranes. Based on such a mode, one hypothesis could be that water transport across the membranes occurs via the H-bonding networks between water molecules and the hydrophilic residues in the pore wall (Figure 4C-4D). TEM analysis of **H2OC1** under conditions similar to those of crystallization revealed extended fiber assembly with external diameter of about 20.6 nm (Figure S22A). These fibers may be formed of five to six channel units across its diameter. In contrast, **H2OC2** fiber bundles are about 9.3 nm in diameter (Figure S22B).

## All-atom molecular dynamics (MD) simulations

To gain molecular insights into the dynamics of **H2OC1** channel in the lipid bilayer, we performed explicitly solvated all atom MD simulations. We used the experimental crystal structure of the **H2OC1** channel composed of 8 monomeric helices as well as 16 kinked **H2OC1** oligourea helices positioned on the side of the channel. We embedded this

construct in a POPC: POPS (4:1 ratio; POPC: 1-palmitoyl-2-oleoyl-sn-glycero-3-phosphocholine, POPS: palmitoyl-oleoyl phosphatidylserine) lipid bilayer (Figure 5Ai). After 200 ns of the equilibration simulation with restrained alpha carbon positions of all helical oligoureas only, we observed that 12 kinked peptides that were positioned between lipid head groups of the membrane remained bound to the channel (Figure 5Aii), while those above or below dissociated.

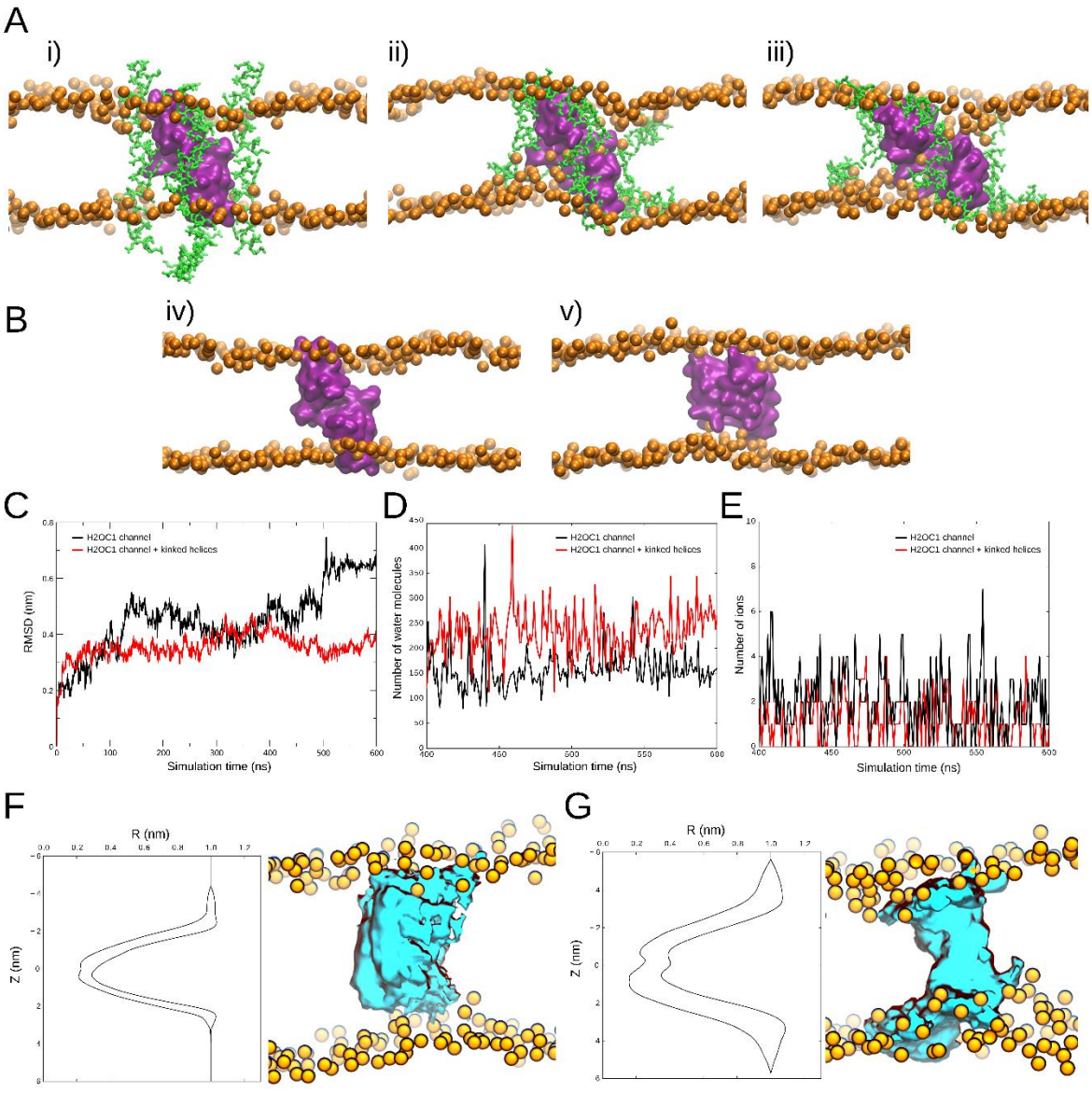


**Figure 5. Molecular dynamics simulations of H2OC1 oligourea channel in POPC:POPS (4:1 ratio) lipid bilayer**

(A) The **H2OC1** oligourea channel composed of 8 helical and 16 kinked helices embedded in lipid bilayer together with simulation snapshots: i) prior to any simulation, ii) after 200 ns of equilibration with position restraints on helical foldamer alpha carbon atoms, iii) after 600 ns of the production run without any restraints. Surface representation of the helices are shown in purple. The 16 kinked helices are shown in green licorice representation. Orange spheres correspond to phospholipid head groups. Water, ions and lipid headgroups were omitted for figure clarity.
(B) Control system of the **H2OC1** oligourea channel composed of 8 helices alone together with simulation snapshots: iv) after 200 ns of equilibration with position restraints on alpha carbon atoms, v) after 600 ns of the production run without any restraints.
(C) Root mean-square-deviation (RMSD) of alpha carbon atoms from 8 helices calculated with respect to the experimental structure.
(D and E) Number of water molecules (D) and number of ions (E) passing through both channel types (shown in A and B) over the last 200 ns of the trajectory are shown.
(F and G) Average channel radius profile across the membrane normal (the two radius profile tracings in each represent the standard deviation limits) together with snapshots of the averaged density of the solvent within the pore (blue) are shown for the two cases, namely, with (F) and without kinked (G) helices. The radius profile as well as solvent density were averaged over the last 200 ns of the production run.

After 600 ns of unrestrained production run, the channel retained its supra helical conformation (Figure 5Aiii and Figure S23Movie 1-2) with kinked peptides bound. We also built a control system, which corresponded to **H2OC1** channel composed only of 8 monomeric helices in the same lipid environment (Figure 5Biv). After 200 ns equilibration and 600 ns of the production the supra helix collapsed resembling a closed and cylindrical conformation (Figure 5Bv and Figure S23Movie 3-4). This is indicated by higher root-mean-square deviation (RMSD) of alpha carbons for the system without kinked helices (Figure 5D). Although water molecules were found to permeate through both channels, the **H2OC1** channel with kinked peptides could transport better water molecules (Figure 5D). The longer permeation pathway of **H2OC1** channel with kinked helices allowed formation of more hydrogen bonds between two glutamate-type residues in each oligourea with water molecules (Figure S24A-B). On the other hand, a small fraction of ions could enter both channels, in agreement with our experimental observations (Figure 2E-2I). Averaged radius profiles as well as averaged density of solvent in both channels is shown in Figure 5F-5G. Although both channels have a radius in the membrane center of mass corresponding to ~0.2 nm, indeed, the **H2OC1** channel with kinked peptides has significantly longer permeation pathway. In summary, computer simulations showed that

kinked peptides can stabilize the **H2OC1** channel, which allows more water molecules to permeate through the membrane.

## Conclusions

We have successfully designed and synthesized oligourea foldamers that form superhelical water channels in aqueous condition stabilized by hydrophobic and electrostatic interactions. Oligourea foldamers **H2OC1** and **H2OC2** showed significant water permeability with high salt rejection in liposomes. In contrast, **H2OC3** and **H2OC4** showed permeability to ions along with water in liposomes. A high-resolution crystal structure of **H2OC1** revealed that salt-bridges facilitate intricate H-bonding network among proximal and distal oligourea residues to stabilize the packing that was confirmed by the formation of fibers of the same dimension that were observed by TEM. Solid-state NMR and cryo-EM data suggest stable insertion of foldamers without perturbing the liposomes. The design-of the amphiphilic foldamers results in the formation of self-assembled tertiary structures conferring a hydrophobic exterior and hydrophilic interior lumen filled with H-bonded water clusters. It results in high water permeability across lipid membranes. Therefore, such oligourea foldamers that are similar to natural porin-like structures are potential candidates for fabrication of AWC membranes for water purification applications.

Unlike the previously described AWCs, our foldamers laterally self-assemble to form the channel. This represents a novel design strategy of using short (10-residue) oligourea foldamers for AWCs and other channels/transporters. We could achieve distinct water and ion permeabilities by altering the sequences of foldamers. The de novo design described herein has potential advantages. Changing the hydrophobic and hydrophilic surfaces of these foldamers allows self-assembly of channels with different diameters and water/ion permeabilities. The design strategy of incorporating polar and nonpolar side chains within the channel lumen could allow selective interactions and transport of cations, anions and water. This highlights the versatility and potential of such oligourea foldamers for systematic and rational design to achieve different structural and functional properties.

# EXPERIMENTAL PROCEDURES

## Resource availability

### Lead contact

Further information and requests for resources and reagents should be directed to and will be fulfilled by the lead contacts, Prakash Kumar (prakash.kumar@nus.edu.sg); R. M. Kini (dbskinim@nus.edu.sg) and Gilles Guichard (g.guichard@iecb.u-bordeaux.fr); Mihail Barboiu (mihail-dumitru.barboiu@umontpellier.fr).

### Materials availability

Unique reagents generated in this study are available from the lead contacts with a completed material transfer agreement.

## SUPPLEMENTAL INFORMATION

Supplemental information can be found online at: <provide url after publication>

## ACKNOWLEDGEMENTS

This research was supported by the National Research Foundation, Singapore, and PUB, Singapore's National Water Agency under its Competitive Research Programme, CRP (Water) (1601-CRPW-T21). G.G. and M.B. acknowledge support from the CNRS through the MITI interdisciplinary programs (Défi Biomimetisme 2019 and 2020). This work was also partly supported by the Agence Nationale de la Recherche (ANR) grants ANR-17-CE07-0020 and ANR-18-CE06-0004-02, WATERCHANNELS. A postdoctoral fellowship to S.H.Yoo from IdEx Bordeaux (ANR-10-IDEX-03-02), a program of the French government managed by the ANR is gratefully acknowledged. This work has benefited from the Biophysical and Structural Chemistry Platform at IECB, CNRS UAR 3033, INSERM US001. Mr. Choong Yeu Khai provided technical help in X-ray data collection.

D. Su appreciates receiving a scholarship from China Scholarship Council as support at University of Montpellier, France.

## AUTHOR CONTRIBUTIONS

G.G., R.M.K, P.P.K., C.D. devised the project; C.D., G.G., S.H.Y., M.P, P.K. designed and synthesized the molecular structures, carried out the experimental work; C.D.

obtained the crystals and diffraction data; G.W.C. solved and refined the crystal structure; A.L and A.G. designed and performed ssNMR experiments; J.L., M.L., performed cryo-EM studies; D.S., M.B. carried out patch-clamp work and verified liposome assays; J.K.M., P.J.B., C.V. carried out the MD simulation work; C.D., G.G., G.W.C., A. L., M.B., R.M.K, P.P.K., analyzed the experimental data; All authors participated in manuscript writing and editing; Funding acquisition and supervision by G.G., M.B., R.M.K, P.P.K.

## DECLARATION OF INTERESTS

C.D., P.K., D.S., S.H.Y., G.G., M.B., R.M.K, P.P.K. are inventors on a patent application related to this work.

## REFERENCES


1. Porter, C.J., Werber, J.R., Zhong, M., Wilson, C.J., and Elimelech, M. (2020). Pathways and challenges for biomimetic desalination membranes with sub-nanometer channels. ACS Nano *14*, 10894–10916.
2. Barboiu, M., and Gilles, A. (2013). From natural to bioassisted and biomimetic artificial water channel systems. Acc. Chem. Res. *46*, 2814–2823.
3. Murata, K., Mitsuoka, K., Hiral, T., Walz, T., Agre, P., Heymann, J.B., Engel, A., and Fujiyoshi, Y. (2000). Structural determinants of water permeation through aquaporin-1. Nature *407*, 599–605.
4. Yuan, Y. Di, Dong, J., Liu, J., Zhao, D., Wu, H., Zhou, W., Gan, H.X., Tong, Y.W., Jiang, J., and Zhao, D. (2020). Porous organic cages as synthetic water channels. Nat. Commun. *11*, 3–12.
5. Tunuguntla, R.H., Henley, R.Y., Yao, Y.-C., Pham, T.A., Wanunu, M., and Noy, A. (2017). Enhanced water permeability and tunable ion selectivity in subnanometer carbon nanotube porins. Science *357*, 792–796.
6. Li, Y., Li, Z., Aydin, F., Quan, J., Chen, X., Yao, Y.C., Zhan, C., Chen, Y., Pham,

T.A., and Noy, A. (2020). Water-ion permselectivity of narrow-diameter carbon nanotubes. Sci. Adv. *6*, eaba9966

7. Leduc, Y., Michau, M., Gilles, A., Gence, V., Legrand, Y.M., Vanderlee, A., Tingry, S., and Barboiu, M. (2011). Imidazole-quartet water and proton dipolar channels. Angew. Chem. Int. Ed. *50*, 11366–11372.
8. Licsandru, E., Kocsis, I., Shen, Y.X., Murail, S., Legrand, Y.M., Van Der Lee, A., Tsai, D., Baaden, M., Kumar, M., and Barboiu, M. (2016). Salt-excluding artificial water channels exhibiting enhanced dipolar water and proton translocation. J. Am. Chem. Soc. *138*, 5403–5409.
9. Huang, L.-B., Di Vincenzo, M., Ahunbay, M.G., van der Lee, A., Cot, D., Cerneaux, S., Maurin, G., and Barboiu, M. (2021). Bilayer versus polymeric artificial water channel membranes: structural determinants for enhanced filtration performances. J. Am. Chem. Soc. *143*, 14386–14393.
10. Di Vincenzo, M., Tiraferri, A., Musteata, V.-E., Chisca, S., Sougrat, R., Huang, L.-B., Nunes, S.P., and Barboiu, M. (2021). Biomimetic artificial water channel membranes for enhanced desalination. Nat. Nanotechnol. *16*, 190–196.
11. Itoh, Y., Chen, S., Hirahara, R., Konda, T., Aoki, T., Ueda, T., Shimada, I., Cannon, J.J., Shao, C., Shiomi, J., et al. (2022). Ultrafast water permeation through nanochannels with a densely fluorous interior surface. Science *376*, 738–743.
12. Hu, X., Chen, Z., Tang, G., Hou, J., and Li, Z. (2012). Single-molecular artificial transmembrane water channels. *1*, 10–13.
13. Shen, Y.X., Si, W., Erbakan, M., Decker, K., De Zorzi, R., Saboe, P.O., Kang, Y.J., Majd, S., Butler, P.J., Walz, T., et al. (2015). Highly permeable artificial water channels that can self-assemble into two-dimensional arrays. Proc. Natl. Acad. Sci. U. S. A. *112*, 9810–9815.
14. Song, W., Joshi, H., Chowdhury, R., Najem, J.S., Shen, Y.X., Lang, C., Henderson, C.B., Tu, Y.M., Farell, M., Pitz, M.E., et al. (2020). Artificial water channels enable fast and selective water permeation through water-wire networks. Nat. Nanotechnol. *15*, 73–79.
15. Lang, C., Deng, X., Yang, F., Yang, B., Wang, W., Qi, S., Zhang, X., Zhang, C., Dong, Z., and Liu, J. (2017). Highly selective artificial potassium ion channels

constructed from pore-containing helical oligomers. Angew. Chem. Int. Ed. *56*, 12668–12671.

16. Zhu, J., Dong, Z., Lei, S., Cao, L., Yang, B., Li, W., Zhang, Y., Liu, J., and Shen, J. (2015). Design of aromatic helical polymers for STM visualization: Imaging of single and double helices with a pattern of π-π stacking. Angew. Chem. Int. Ed. *54*, 3097–3101.
17. Lang, C., Li, W., Dong, Z., Zhang, X., Yang, F., Yang, B., Deng, X., Zhang, C., Xu, J., and Liu, J. (2016). Biomimetic transmembrane channels with high stability and transporting efficiency from helically folded macromolecules. Angew. Chem.Int. Ed. *55*, 9723–9727.
18. Huo, Y., and Zeng, H. (2016). "Sticky"-ends-guided creation of functional hollow nanopores for guest encapsulation and water transport. Acc. Chem. Res. *49*, 922–930.
19. Shen, J., Fan, J., Ye, R., Li, N., Mu, Y., and Zeng, H. (2020). Polypyridine- based helical amide foldamer channels: rapid transport of water and protons with high ion rejection. Angew. Chem. Int. Ed. *59*, 13328–13334.
20. Roy, A., Shen, J., Joshi, H., Song, W., Tu, Y.M., Chowdhury, R., Ye, R., Li, N., Ren, C., Kumar, M., et al. (2021). Foldamer-based ultrapermeable and highly selective artificial water channels that exclude protons. Nat. Nanotechnol. *16*, 911–917.
21. Shen, J., Roy, A., Joshi, H., Samineni, L., Ye, R., Tu, Y.-M., Song, W., Skiles, M., Kumar, M., Aksimentiev, A., et al. (2022). Fluorofoldamer-based salt- and proton-rejecting artificial water channels for ultrafast water transport. Nano Lett. *22*, 4831–4838.
22. Yoo, S.H., Li, B., Dolain, C., Pasco, M., and Guichard, G. (2021). Urea based foldamers. Methods Enzymol. *656*, 59–92.
23. Collie, G.W., Pulka-Ziach, K., Lombardo, C.M., Fremaux, J., Rosu, F., Decossas, M., Mauran, L., Lambert, O., Gabelica, V., Mackereth, C.D., et al. (2015). Shaping quaternary assemblies of water-soluble non-peptide helical foldamers by sequence manipulation. Nat. Chem. *7*, 871–878.
24. Yoo, S.H., Collie, G.W., Mauran, L., and Guichard, G. (2020). Formation and

modulation of nanotubular assemblies of oligourea foldamers in aqueous conditions using alcohol additives. Chempluschem *85*, 2243–2250.

25. Collie, G.W., Lombardo, C.M., Yoo, S.H., Pułka-Ziach, K., Gabelica, V., Mackereth, C.D., Rosu, F., and Guichard, G. (2021). Crystal structures capture multiple stoichiometric states of an aqueous self-assembling oligourea foldamer. Chem. Commun. *57*, 9514–9517.
26. Douat-Casassus, C., Pulka, K., Claudon, P., and Guichard, G. (2012). Microwave-enhanced solid-phase synthesis of N,N′-linked aliphatic oligoureas and related hybrids. Org. Lett. *14*, 3130–3133.
27. Teyssières, E., Corre, J.P., Antunes, S., Rougeot, C., Dugave, C., Jouvion, G., Claudon, P., Mikaty, G., Douat, C., Goossens, P.L., et al. (2016). Proteolytically stable foldamer mimics of host-defense peptides with protective activities in a murine model of bacterial infection. J. Med. Chem. *59*, 8221–8232.
28. Snook, C., Woolley, G., Oliva, G., Pattabhi, V., Wood, S., Blundell, T., and Wallace, B. (1998). The structure and function of antiamoebin I, a proline-rich membrane-active polypeptide. Structure *6*, 783–792.
29. Portella, G., and de Groot, B.L. (2009). Determinants of water permeability through nanoscopic hydrophilic channels. Biophys. J. *96*, 925–938.
30. Mishra, V.K., Palgunachari, M.N., Krishna, N.R., Glushka, J., Segrest, J.P., and Anantharamaiah, G.M. (2008). Effect of leucine to phenylalanine substitution on the nonpolar face of a class A amphipathic helical peptide on its interaction with lipid: High resolution solution NMR studies of 4F-dimyristoylphosphatidylcholine discoidal complex. J. Biol. Chem. *283*, 34393–34402.
31. Lombardo, C.M., Collie, G.W., Pulka-Ziach, K., Rosu, F., Gabelica, V., Mackereth, C.D., and Guichard, G. (2016). Anatomy of an oligourea six-helix bundle. J. Am. Chem. Soc. *138*, 10522–10530.
32. Roy, A., Shen, J., Joshi, H., Song, W., Tu, Y.M., Chowdhury, R., Ye, R., Li, N., Ren, C., Kumar, M., et al. (2021). Foldamer-based ultrapermeable and highly selective artificial water channels that exclude protons. Nat. Nanotechnol. *16*, 911–917.
33. Shen, J., Ye, R., Romanies, A., Roy, A., Chen, F., Ren, C., Liu, Z., and Zeng, H.

(2020). Aquafoldmer-based aquaporin-like synthetic water channel. J. Am. Chem. Soc. *142*, 10050–10058.

34. Shen, Y.X., Song, W.C., Ryan Barden, D., Ren, T., Lang, C., Feroz, H., Henderson, C.B., Saboe, P.O., Tsai, D., Yan, H., et al. (2018). Achieving high permeability and enhanced selectivity for Angstrom-scale separations using artificial water channel membranes. Nat. Commun. *9*, 1–11.
35. Barboiu, M., Le Duc, Y., Gilles, A., Cazade, P.A., Michau, M., Marie Legrand, Y., Van Der Lee, A., Coasne, B., Parvizi, P., Post, J., et al. (2014). An artificial primitive mimic of the Gramicidin-A channel. Nat. Commun. *5*, 2–9.
36. Leite, N.B., Aufderhorst-Roberts, A., Palma, M.S., Connell, S.D., Neto, J.R., and Beales, P.A. (2015). PE and PS lipids synergistically enhance membrane poration by a peptide with anticancer properties. Biophys. J. *109*, 936–947.
37. Rusinova, R., Kim, D.M., Nimigean, C.M., and Andersen, O.S. (2014). Regulation of ion channel function by the host lipid bilayer examined by a stopped-flow spectrofluorometric assay. Biophys. J. *106*, 1070–1078.
38. Posson, D.J., Rusinova, R., Andersen, O.S., and Nimigean, C.M. (2018). Stopped-flow fluorometric ion flux assay for ligand-gated ion channel studies. Methods Mol Biol. 1684, 223–235.
39. Lee, K.C.B., Siegel, J., Webb, S.E.D., Lévêque-Fort, S., Cole, M.J., Jones, R., Dowling, K., Lever, M.J., and French, P.M.W. (2001). Application of the stretched exponential function to fluorescence lifetime imaging. Biophys. J. *81*, 1265–1274.
40. Saha, T., Gautam, A., Mukherjee, A., Lahiri, M., and Talukdar, P. (2016). Chloride transport through supramolecular barrel-rosette ion channels: lipophilic control and apoptosis-inducing activity. J. Am. Chem. Soc. *138*, 16443–16451.
41. Ren, C., Zeng, F., Shen, J., Chen, F., Roy, A., Zhou, S., Ren, H., and Zeng, H. (2018). Pore-forming monopeptides as exceptionally active anion channels. J. Am. Chem. Soc. *140*, 8817–8826.
42. Schneider, S., Licsandru, E.D., Kocsis, I., Gilles, A., Dumitru, F., Moulin, E., Tan, J., Lehn, J.M., Giuseppone, N., and Barboiu, M. (2017). Columnar self-assemblies of triarylamines as scaffolds for artificial biomimetic channels for ion and for water transport. J. Am. Chem. Soc. *139*, 3721–3727.